Classification
Physics Abstracts
46.60B — 47.15F — 47.60

Flow induced instability of the interface between a fluid and a gel at low Reynolds number

V. Kumaran, G. H. Fredrickson and P. Pincus

Department of Chemical and Nuclear Engineering and Materials Department, University of California, Santa Barbara, CA 93106, U.S.A.

(Received 10 October 1993, received in final form 28 December 1993, accepted 21 February 1994)

Abstract. — The stability of the interface between a gel of thickness HR and a Newtonian fluid of thickness R subjected to a linear shear flow is studied in the limit where inertial effects are negligible. The shear stress for the gel contains an elastic part that depends on the local displacement field and a viscous component that depends on the velocity field. The shear flow at the surface tends to destabilize the surface fluctuations, and the critical strain rate γ_c, which is the minimum strain rate required for unstable fluctuations, is determined as a function of the dimensionless quantities H, $\eta_r = (\eta_g/\eta_f)$, and $T = (\Gamma/ER)$. Here η_g and η_f are the gel and fluid viscosities, E is the gel elasticity, Γ is the surface tension of the gel — fluid interface and the strain rate γ is scaled by (E/η_f). In the limit $H \to \infty$, we find that γ_c decreases proportional to H^{-1} independent of η_r and T. But at finite H, γ_c is strongly dependent on η_r and T. For $\eta_r \geq 1$, the interface is stable for all values of the strain rate for $H < \sqrt{\eta_r}$, while there are unstable traveling waves for $H > \sqrt{\eta_r}$. For $\eta_r = 1$ and $H \to 1$, we find that $\gamma_c \propto (H-1)^{-1/2}$ for $T = 0$ and $\gamma_c \propto (H-1)^{-3/4} T^{1/4}$ for $T \neq 0$. For $\eta_r > 1$, the analysis indicates that $\gamma_c \propto (H - \sqrt{\eta_r})^{-1}$ independent of T for $H \to \sqrt{\eta_r}$. For $\eta_r < 1$, the onset of instability depends strongly on the parameter T. For $T = 0$, the critical strain rate is finite in the limit $H \to 0$, while for $T \neq 0$ the critical strain rate diverges at a finite value of H. This minimum H decreases proportional to η_r for large T. The instability is caused by the energy transfer from the mean flow to the fluctuations due to the work done by the mean flow at the interface.

1. Introduction.

Recent experimental observations indicate that fluid flow past a flexible surface induces oscillations in the surface, and these oscillations change the characteristics of the flow. Silberberg [1] and coworkers studied the flow of a Newtonian fluid through tubes with gel coated walls. They observed that the pressure drop required to maintain the flow is significantly higher than that required for rigid walled tubes, even at Reynolds numbers well below the transition Reynolds number at which the fluid becomes turbulent. This increased

drag was attributed to an increase in the viscous dissipation of energy due to oscillations of the walls of the tube. More recently, Klein, Perahia and Warburg [2] studied the effect of shear flow on the surface of a polymer « brush », which consists of polymers end — grafted onto a solid surface. They used a surface force apparatus in which polymer molecules were grafted onto the two surfaces, and the surfaces were sheared past each other. An anomalous normal force between the surfaces was observed as the velocity of the surfaces was increased, and this was interpreted as an increase in the brush thickness, which may be due to the growth of surface waves. In this paper, we use a linear stability analysis to determine the stability of the interface between a linear viscoelastic gel and a Newtonian fluid under shear flow. A better understanding of the factors that influence the interfacial stability would be useful for explaining experimental observations, and would also be relevant for practical applications such as polymer tribilogy and biotransport which involve flows past flexible surfaces.

It is well-known that the interface between two Newtonian fluids becomes unstable when the Reynolds number exceeds a critical value. The fluid inertia is necessary to induce the instability in Newtonian fluids, since the equations are not explicitly time dependent if the inertial terms are neglected. The stability of a film of a second order model of a fluid flowing down an inclined surface was studied by Gupta [3] and Shaqfeh *et al.* [4]. It was found that the viscoelasticity destabilises the interface between the fluids, and the critical Reynolds number for a second order fluid is lower than that for a Newtonian fluid. There has been considerable work done on the instability due to viscosity or density stratification in a fluid. Yih [5] and Hooper and Boyd [6] showed that there is an instability between two Newtonian fluids at non-zero Reynolds number due to viscosity stratification, and Waters and Keely [7] and Renardy [8] generalized this to Oldroyd-B and upper convected Maxwell fluids respectively. Chen [9] subsequently showed that there is an elastic instability at the interface between the two non-Newtonian fluids even in the absence of viscosity stratification due to a jump in the first normal stress across the surface in the base flow.

Here we analyse the stability of the interface between an elastic gel and a Newtonian fluid when a shear flow is applied to the fluid. The inertia of the fluid and gel are neglected in the analysis, and there is no normal stress difference across the surface which causes the elastic instabilities observed in previous studies [9]. We find that the interface becomes unstable when the strain rate in the fluid exceeds a critical value which depends on the ratio of the gel and fluid thickness H, the ratio of the fluid and gel viscosities $\eta_r = (\eta_g/\eta_f)$ and a dimensionless number $T = (\Gamma/RE)$ which is the ratio of the forces due to the surface tension Γ of the fluid — gel interface and the elastic stress in the gel. The instability is driven by the energy transfer from the mean flow to the fluctuations due to the work done by the mean flow at the interface. We find that there is much variety in the characteristics of the instability due to variations in η_r and T. Specifically, the characteristics of the instability are independent of η_r and T for $H \gg 1$, but for $H \sim 1$ we find that the most unstable mode has qualitatively different features for $\eta_r > 1$, $\eta_r = 1$ and $\eta_r < 1$. This variety in the behaviour would not be captured by less detailed analyses which represent the dynamics of the gel using a constitutive equation. The theoretical predictions are in qualitative agreement the experimental observations of Krindel and Silberberg [18] in the limit $H \gg 1$.

2. Model.

The system consists of an elastic gel of thickness HR fixed onto a surface at $z = -HR$, and a layer of fluid of thickness R in the region $0 < z < R$. The fluid is bounded by a solid wall, which moves at a constant velocity V in the x direction relative to the gel as shown in figure 1. Small perturbations to the interface are induced by spontaneous fluctuations, and we study the effect of the fluid flow on the growth of these perturbations.

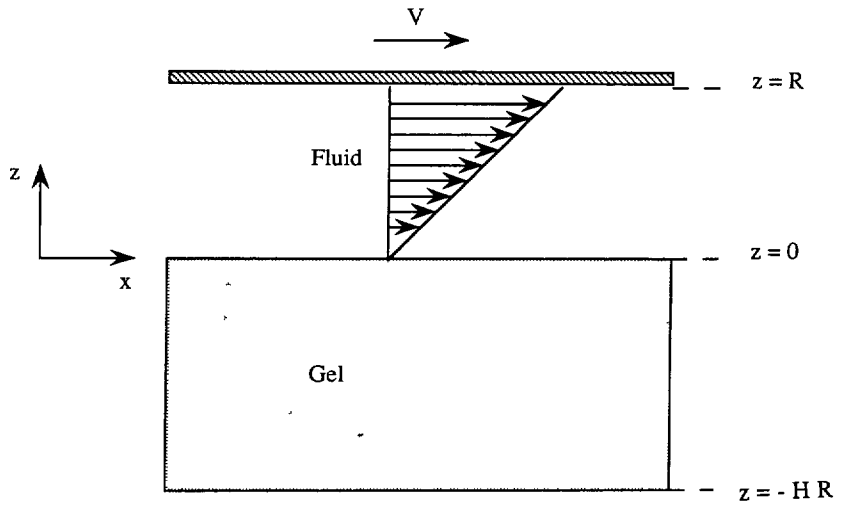

Fig. 1. — Schematic of the configuration and fluid velocity field.

The gel is at rest in the unperturbed state, and the dynamical fluctuations in the gel are characterized by a displacement field **u** which represents the displacement of the material points from their equilibrium positions. The gel is considered to be incompressible and impermeable to the fluid, so that the displacement field satisfies the following incompressibility condition :

$$\nabla \cdot \mathbf{u} = 0 . \tag{1}$$

The momentum conservation equation for the gel is :

$$\rho \left(\frac{\partial^2 \mathbf{u}}{\partial t^2} \right) = - \nabla p + E \nabla^2 \mathbf{u} + \eta_g \nabla^2 \frac{\partial \mathbf{u}}{\partial t} \tag{2}$$

and the stress in the gel is given by :

$$\sigma_{ij} = - p \delta_{ij} + \left(E + \eta_g \frac{\partial}{\partial t} \right) \left(\frac{\partial u_i}{\partial x_j} + \frac{\partial u_j}{\partial x_i} \right) \tag{3}$$

where ρ is the density, E is the coefficient of elasticity and η_g is the viscosity of the gel. In (2), the left side is the rate of change of momentum, the first term on the right side is the gradient of the pressure which is required to enforce incompressibility, the second term on the right side is the elastic stress due to the strain an incompressible gel [10] and the last term is the usual viscous stress due to the gradients in the velocity. Equation (2) has been used previously in literature for polymer gels [11, 13], and equations similar to this have been used in the studies of flow past compliant media [14-16]. Since the gel is fixed to a solid surface, the appropriate boundary conditions at $z = - HR$ are :

$$u_z = 0 \quad u_x = 0 . \tag{4}$$

The conservation equations, (1) and (2), along with the boundary conditions at the interface and at $z = - HR$, can be solved to obtain the displacement and pressure fields in the gel.

The flow of the fluid is governed by the Navier-Stokes mass and momentum conservation equations. In the absence of fluid inertia, the conservation equations are :

$$\nabla \cdot \mathbf{v} = 0 \tag{5}$$

$$\nabla \cdot \boldsymbol{\tau} = 0 \tag{6}$$

where $\boldsymbol{\tau}$, the fluid stress tensor, has the usual form :

$$\tau_{ij} = -p\delta_{ij} + \eta_f \left(\frac{\partial v_i}{\partial x_j} + \frac{\partial v_j}{\partial x_i} \right) \tag{7}$$

where η_f is the fluid viscosity. Note that we use the symbol $\boldsymbol{\sigma}$ for the stress tensor in the gel, and the symbol $\boldsymbol{\tau}$ for the stress tensor in the fluid. No-slip boundary conditions are appropriate at $z = R$:

$$v_x = V \quad v_z = 0 \,. \tag{8}$$

The mean flow in the fluid is a Couette flow with a no-slip boundary condition at the surface :

$$v_{x0} = \frac{Vz}{R} \tag{9}$$

and the boundary conditions at the interface between the fluid and the gel are the usual continuity of velocity and stress :

$$\frac{\partial u_x}{\partial t} = v_x \quad \frac{\partial u_z}{\partial t} = v_z \tag{10}$$

$$\sigma_{xz} = \tau_{xz} \quad \sigma_{zz} = \tau_{zz} + \Gamma \frac{\partial^2 u_z}{\partial x^2} \,. \tag{11}$$

The last term on the right side of the normal stress conservation equation is the stress due to the surface tension when there is a small displacement u_z of the surface about its equilibrium state $z = 0$. In previous studies of the interfacial instability between upper convected Maxwell fluids [9] it has been pointed out that there is an additional term in the shear stress boundary condition (11) due to the discontinuity in the first normal stress difference across the surface in the base state. This term is proportional to the relaxation time and the square of the strain rate of the fluids. In our system, the fluid in the channel is Newtonian and its relaxation time is zero, while the gel has zero velocity in the base state, and therefore we do not have this additional term in the stress balance equation.

The length scales in the conservation equations (1) and (2) are scaled by R and the time scales by (η_f/E). The scaled conservation equations for the displacement field in the gel :

$$\nabla \cdot \mathbf{u} = 0 \tag{12}$$

$$-\nabla p + \nabla^2 \mathbf{u} + \eta_r \nabla^2 \left(\frac{\partial \mathbf{u}}{\partial t} \right) = 0 \tag{13}$$

where $\eta_r = (\eta_g/\eta_f)$ is the ratio of the gel and fluid viscosities, and the pressure p is non-dimensionalised by E. The scaled shear and normal stresses in the gel are given by :

$$\sigma_{zz} = -p + 2\left(1 + \eta_r \frac{\partial}{\partial t}\right)\left(\frac{\partial u_z}{\partial z}\right) \tag{14}$$

$$\sigma_{xz} = \left(1 + \eta_r \frac{\partial}{\partial t}\right)\left(\frac{\partial u_z}{\partial x} + \frac{\partial u_x}{\partial z}\right) . \tag{15}$$

The length scales in the fluid are non-dimensionalised by R, and the velocities by (RE/η_f) :

$$\nabla \cdot \mathbf{v} = 0 \tag{16}$$

$$-\nabla p + \nabla^2 \mathbf{v} = 0 . \tag{17}$$

The normal and shear stresses are scaled by the shear modulus, E :

$$\tau_{zz} = -p + 2\left(\frac{\partial v_z}{\partial z}\right) \tag{18}$$

$$\tau_{xz} = \left(\frac{\partial v_z}{\partial x} + \frac{\partial v_x}{\partial z}\right) . \tag{19}$$

This completes the derivation of the conservation equations for the fluid and the gel, and the appropriate boundary conditions. In the next section the scaled mass and momentum conservation equations, (12), (13), (16) and (17), along with the boundary conditions (10) and (11), are used to analyse the stability of small perturbations at the interface. *From this point onwards, all the variables are scaled unless it is explicitly stated that they are dimensional.*

3. Stability analysis.

In this section, we use a linear stability analysis to calculate the growth rate of small perturbations to the interface between the elastic medium and the fluid. The perturbation to the gel displacement field $\mathbf{u}$ and the fluid velocity field $\mathbf{v}$ are of the form :

$$\mathbf{u} = \tilde{\mathbf{u}}(z)\exp(ikx + \alpha t) \quad \mathbf{v} = \tilde{\mathbf{v}}(z)\exp(ikx + \alpha t) \tag{20}$$

where k is the wave number and α is the growth rate, and the eigenfunctions $\tilde{\mathbf{u}}(z)$ and $\tilde{\mathbf{v}}(z)$ are determined from the conservation equations. Substituting the above expression for $\mathbf{u}$ into the conservation equations (12) and (13), we get the following linearised equations :

$$D\tilde{u}_z + ik\tilde{u}_x = 0 \tag{21}$$

$$-D\tilde{p} + (1 + \eta_r \alpha)(D^2 - k^2)\tilde{u}_z = 0 \tag{22}$$

$$-ik\tilde{p} + (1 + \eta_r \alpha)(D^2 - k^2)\tilde{u}_x = 0 \tag{23}$$

where D represents $\partial/\partial z$, and $\tilde{p}$ is the perturbation to the pressure field in the gel. The linearised equation for the fluid velocity field is calculated by substituting (20) into (16) and (17) :

$$D\tilde{v}_z + ikv_x = 0 \tag{24}$$

$$-D\tilde{p} + (D^2 - k^2)\tilde{v}_z = 0 \tag{25}$$

$$-ik\tilde{p} + (D^2 - k^2)\tilde{v}_x = 0 . \tag{26}$$

The perturbations to the stress fields in the gel, $\tilde{\sigma}$, and fluid, $\tilde{\tau}$, are calculated from (14), (15), (18) and (19) :

$$\tilde{\sigma}_{zz} = -\tilde{p} + 2(1 + \eta_r \alpha) D\tilde{u}_z \quad \tilde{\sigma}_{xz} = (1 + \eta_r \alpha)(ik\tilde{u}_z + D\tilde{u}_x) \tag{27}$$

$$\tilde{\tau}_{zz} = -\tilde{p} + 2D\tilde{v}_z \quad \tilde{\tau}_{xz} = (ik\tilde{v}_z + D\tilde{v}_x) . \tag{28}$$

Finally, the boundary conditions for the perturbations to the velocity field (10) at the interface $(z = h(x))$ is :

$$\tilde{v}_z = \alpha\tilde{u}_z \quad \tilde{v}_x + \gamma\tilde{u}_z = \alpha\tilde{u}_x . \tag{29}$$

There is a term proportional to the non-dimensional strain rate in the fluid, $\gamma \equiv (V\eta_f/(ER))$, in the boundary condition for v_x due to the mean flow velocity gradient in the fluid at the interface. In this term, we have approximated the height of the interface, $h(x)$, by the displacement u_z at $z = 0$, which is permissible for small perturbations. This term is the only connection between the base flow and the perturbations, and is responsible for inducing the surface instabilities that we discuss further on. Finally, we have the matching stress conditions at the interface (11) :

$$\tilde{\tau}_{zz} - Tk^2\,\tilde{u}_z = \tilde{\sigma}_{zz} \quad \tilde{\tau}_{xz} = \tilde{\sigma}_{xz} \tag{30}$$

where $T = (\Gamma/ER)$ is the ratio of the surface tension and elastic stresses.

The eigen functions $\tilde{\mathbf{u}}(z)$ for the displacement field $\mathbf{u}$ are calculated by solving the conservation equations, (21), (22) and (23) :

$$\begin{pmatrix} \tilde{u}_z \\ \tilde{u}_x \end{pmatrix} = A \begin{pmatrix} \exp(kz) \\ (kz)\exp(kz) \\ \exp(-kz) \\ (kz)\exp(-kz) \end{pmatrix} \tag{31}$$

where A is a 2×4 matrix of complex coefficients. In this matrix there are four independent coefficients ; the others are fixed by the conservation equations. Two of the coefficients are determined from the displacement boundary conditions at $z = -HR$ (4), while the others are determined from the matching conditions at the interface between the fluid and the gel.

The eigen functions for the fluid flow above the interface are determined from the fluid conservation equations (24), (25) and (26), and are similar to the eigen functions for the displacement field :

$$\begin{pmatrix} \tilde{v}_z \\ \tilde{v}_x \end{pmatrix} = B \begin{pmatrix} \exp(kz) \\ (kz)\exp(kz) \\ \exp(-kz) \\ (kz)\exp(-kz) \end{pmatrix} \tag{32}$$

where B is a 2×4 matrix of complex coefficients, in which all but four of the coefficients are determined by the conservation equations. Two of the coefficients can be expressed in terms of the other two using the boundary conditions at $z = R$, (8). After applying the boundary conditions at $z = -HR$ and $z = R$, we are left with four independent coefficients in the matrices A and B. One of these is arbitrary, because only the relative magnitude of the perturbations is relevant to the analysis, while the other three and the growth rate α are determined from the velocity and stress conditions at the surface of the gel, (29) and (30). After eliminating three of the coefficients, we arrive at a complex characteristic equation which is a quadratic equation for the growth rate α. The detailed calculation of the characteristic equation for the simple case $\eta_r = 1$ is given in the Appendix. This equation is rather complicated and it is difficult to write down the analytical solutions for the two roots, but it is quite easy to calculate them numerically. The behaviour of the more unstable root that has the larger positive real part is analysed in the next section. We note that the behaviour of this root in the different asymptotic regimes (small and large γ and $H - 1 \ll 1$ and $H \gg 1$) were determined by evaluating the root numerically in these regimes, and the scaling laws were obtained from these values. This procedure was found to be simpler than directly expanding the root in a perturbation series due to the complexity of the algebra involved. The stability of the system depends on three dimensionless quantities — the ratio of the gel and fluid thickness H, the ratio of the gel and fluid viscosities $\eta_r = (\eta_g/\eta_f)$ and the dimensionless number $T = (\Gamma/ER)$. We derive the results for the case $\eta_r = 1$ in some detail to illustrate the procedure involved in arriving at the critical strain rate, and state the important results for $\eta_r > 1$ and $\eta_r < 1$.

4. Results.

4.1 $\eta_r = 1$. — First, we present consider the case $\eta_r = 1$ and $T = 0$. The growth rate of the perturbations, α, depends on the ratio of the thicknesses of the fluid and elastic medium, H, and the non-dimensional strain rate at the surface, γ, which is $(V\eta_f/RE)$. We find that in the limit $H \gg 1$ there always exist unstable modes for $\gamma > 0$, whereas for $H < 1$ there are no unstable modes even in the limit $\gamma \to \infty$. The growth rate, frequency and wave number of the fluctuations have the following behaviour in the limits $H \gg 1$, $H = 1$ and in the intermediate regime.

i) In the limit $H \gg 1$, we set $H = \infty$ in the equations of motion, and retain only the modes that decay exponentially into the gel. The real part of the growth rate of the fastest growing mode, α_R, is shown as a function of the wave number k for different values of γ in figure 2. The most unstable mode has a zero growth rate at $\gamma = 0$ and a positive maximum growth rate for all non-zero values of γ, indicating that *there always exist unstable modes* in this limit. Figure 3 shows k_{max}, the wave number of the fastest growing mode as a function of γ. We find that k_{max} increases proportional to $0.5\ \gamma$ for $\gamma \to 0$, reaches a maximum of 0.615 at $\gamma = 6.42$, and then decreases as $1.333\ \gamma^{-2/5}$ for $\gamma \to \infty$. The growth rate of the fastest growing mode, α_R, which is shown in figure 4, increases as $4.1667 \times 10^{-2}\ \gamma^3$ for $\gamma \to 0$, and reaches a maximum value of + 1 for $\gamma \to \infty$. The frequency of the fastest growing mode, $-\alpha_I$, is shown as a function of γ in figure 5. The frequency increases as $0.25\ \gamma^2$ for $\gamma \to 0$, and shows a much slower increase of $1.732\ \gamma^{1/5}$ for $\gamma \to \infty$.

ii) For $H = 1$, the system is marginally stable in the limit $\gamma \to \infty$. The wave number of the mode with the slowest decay rate, k_{max} (Fig. 6), is zero for $\gamma < 4.38$, and increases to a maximum value of 0.919 in the limit $\gamma \to \infty$. Of greater interest is the growth rate, α_R, which is shown in figure 7. This is -0.06699 for $\gamma < 4.38$, and increases as $-4.415/\gamma^2$ in the limit $\gamma \to \infty$. The frequency of the fastest growing mode, $-\alpha_I$, is zero for $\gamma < 4.38$, and increases as $0.1723\ \gamma$ in the limit $k \to \infty$, as shown in figure 8. The scaling of

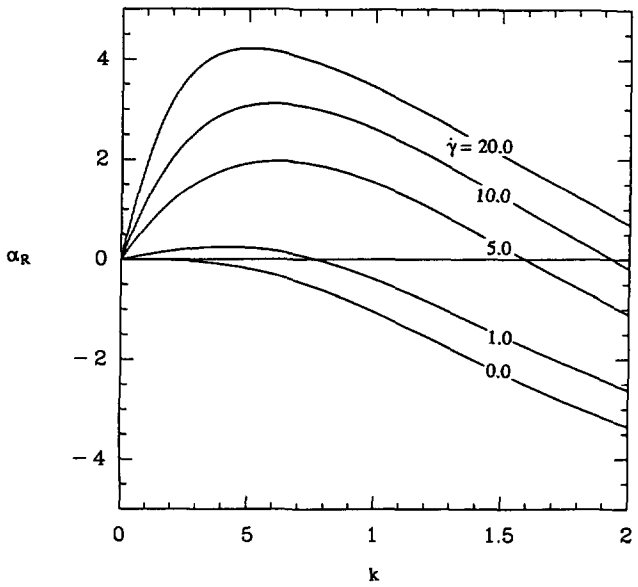

Fig. 2. — Real part of the growth rate, α_R, as a function of the wave number k for $H \gg 1$ for $\eta_r = 1$ and $T = 0$. γ is the mean fluid strain rate.

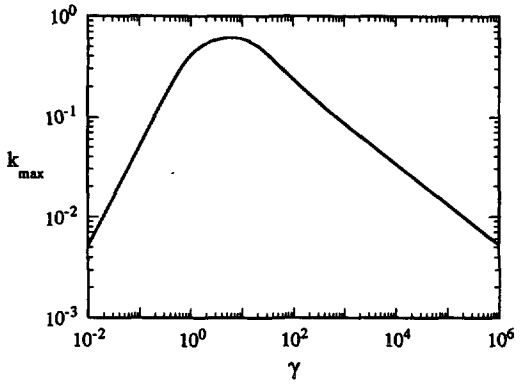

Fig. 3.

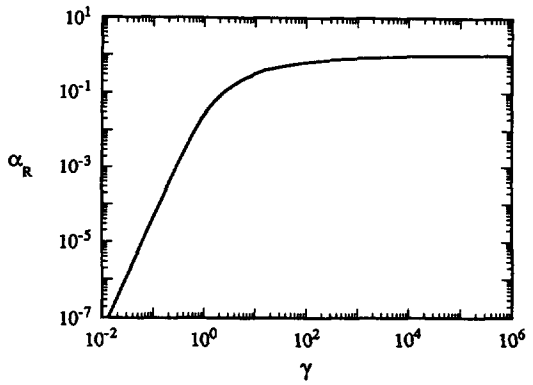

Fig.4.

Fig. 3. — Wave number of the fastest growing mode, k_{max}, as a function of the mean fluid strain rate, γ for $H \gg 1$, $\eta_r = 1$ and $T = 0$.

Fig. 4. — Growth rate of the fastest growing mode, α_R, as a function of the mean fluid strain rate, γ for $H \gg 1$, $\eta_r = 1$ and $T = 0$.

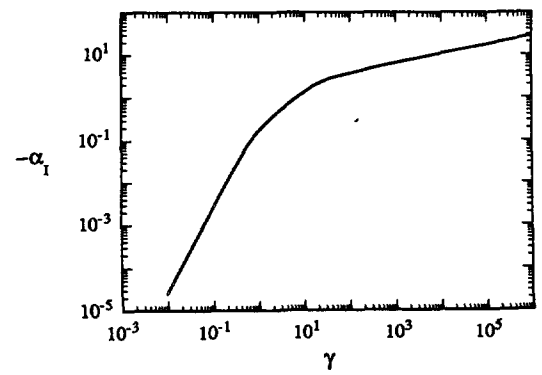

Fig.5.

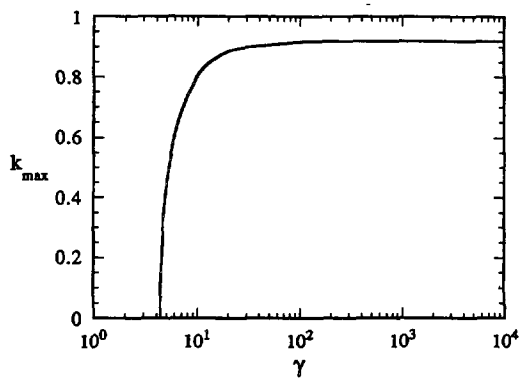

Fig. 6.

Fig. 5. — Frequency of the fastest growing mode, $-\alpha_I$, as a function of the mean fluid strain rate, γ for $H \gg 1$, $\eta_r = 1$ and $T = 0$.

Fig. 6. — Wave number of the mode with the slowest decay rate, k_{max}, as a function of the mean fluid strain rate, γ, for $H = 1$, $\eta_r = 1$ and $T = 0$.

the wave number, growth rate and frequency of the fastest growing modes are summarized in table I.

iii) In the intermediate regime we find that the system is unstable when the strain rate, γ, is greater than a critical value, γ_c. The critical shear rate is shown as a function of the parameter $(H - 1)$ in figure 9 (solid line). The critical strain rate increases as $3.47\,(H-1)^{-1/2}$ in the limit $H \to 1$, and decreases as $3.2\,H^{-1}$ in the limit $H \gg 1$. The wave number of the marginally stable mode at the critical strain rate, k_c (solid line in Fig. 10), is 1.05 for $H \to 1$, and decreases as $1.6\,H^{-1}$ in the limit $H \gg 1$. The frequency of the marginally stable mode, $-\alpha_I$, increases as

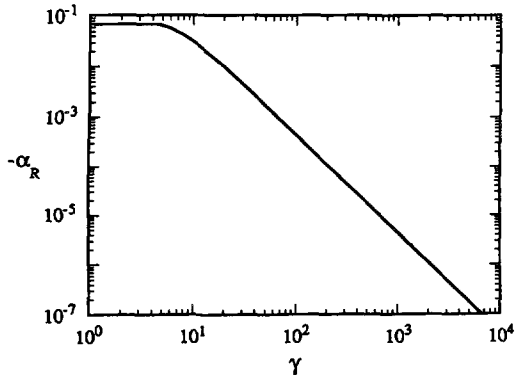

Fig. 7.

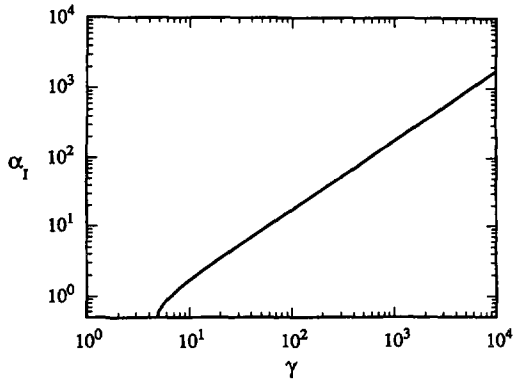

Fig. 8.

Fig. 7. — Decay rate of the mode with the slowest decay rate, $-\alpha_R$, as a function of the mean fluid strain rate, γ, for $H = 1$, $\eta_r = 1$ and $T = 0$.

Fig. 8. — Frequency of the mode with the slowest decay rate, $-\alpha_I$, as a function of the mean fluid strain rate, γ, for $H = 1$, $\eta_r = 1$ and $T = 0$.

Table I. — *The stability, wave number k_{max}, growth rate α_R and frequency $-\alpha_I$ of the fastest growing mode as a function of the strain rate, γ, for $\eta_r = 1$ and $T = 0$.*

Regime	Stability	k_{max}	α_R	$-\alpha_I$
$H \gg 1$ $\gamma \to 0$	Unstable	$0.5\ \gamma$	$4.1667 \times 10^{-2}\ \gamma^3$	$0.25\ \gamma^2$
$H \gg 1$ $\gamma \to \infty$	Unstable	$1.333\ \gamma^{-2/5}$	1.0	$1.732\ \gamma^{1/5}$
$H = 1$ $\gamma \leqslant 4.38$	Stable	0.0	− 0.06699	0.0
$H = 1$ $\gamma \to \infty$	Stable	0.919	$(-4.415\ \gamma^{-2})$	$0.1723\ \gamma$

$0.626(H-1)^{-1/2}$ in the limit $H \to 1$, and decreases as $2.56\ H^{-2}$ in the limit $H \gg 1$, as shown by the solid line in figure 11.

The effect of variation in the surface tension is shown by the broken lines in figures 9, 10 and 11. The surface tension does not affect the behaviour of the critical strain rate in the limit $H \gg 1$, because the unstable modes have wave number $k \to 0$ in this limit and the effect of surface tension decreases as the wavelength increases.

There is a qualitative change in the power law dependence of γ_c on H for $H \sim 1$. The critical strain rate γ_c increases proportional to $T^{1/4}(H-1)^{-3/4}$ (instead of $(H-1)^{-1/2}$ for $T = 0$), and the critical strain rate required to destabilize the surface waves increases as T increases. In addition, we find that the wave number of the marginally stable mode $k_c \propto T^{-1}(H-1)^{1/4}$ (broken lines in Fig. 10), while the frequency of the most unstable mode $-\alpha_I$ is found to be

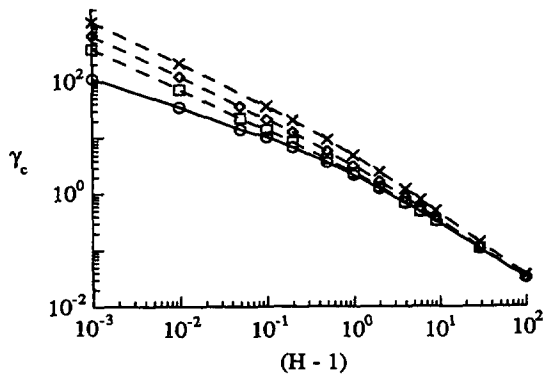

Fig. 9.

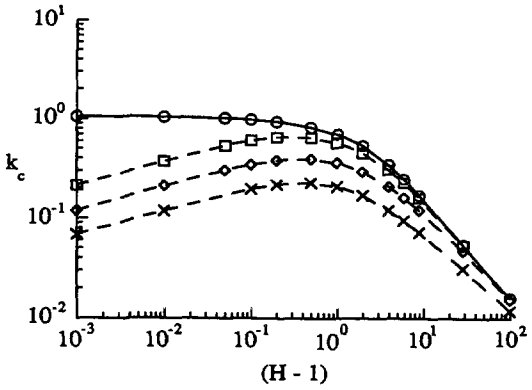

Fig. 10.

Fig. 9. — The critical strain rate, γ_c, required for unstable modes as a function of $(H-1)$ for $\eta_r = 1$. (○) $T = 0$; (□) $T = 1$; (◇) $T = 10$; (×) $T = 100$.

Fig. 10. — Wave number of the marginally stable mode, k_{max}, as a function of $(H-1)$ and $\eta_r = 1$. (○) $T = 0$; (□) $T = 1$; (◇) $T = 10$; (×) $T = 100$.

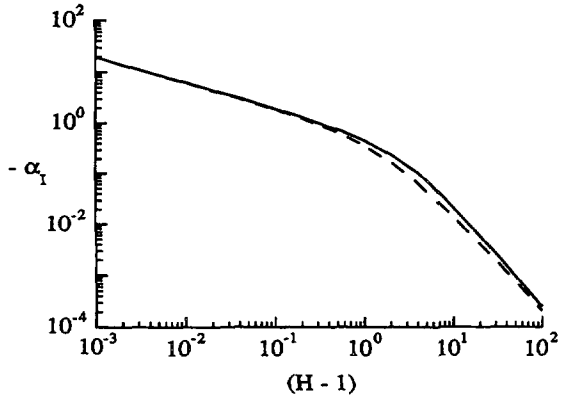

Fig. 11. — Frequency of the marginally stable mode, $-\alpha_I$, as a function of $(H-1)$ and $\eta_r = 1$. (Solid line) $T = 0$; (Broken line) $T = 100$.

independent of T in this limit. The behaviour of the critical strain rate, wave number and frequency are summarized in table II.

4.2 $\eta_r > 1$. — The critical strain rate, γ_c, is shown as a function of H at $T = 0$ and for various values of η_r in figure 12. For $\eta_r > 1$, we see that the critical strain rate diverges at $H = \sqrt{\eta_r}$, and the fluctuations are always stable for $H < \sqrt{\eta_r}$. To analyse this in further detail, we consider the case $\eta_r = 10$ and $T = 0$. The critical strain rate γ_c, the wave number of the fastest growing mode k_c and the frequency of the fastest growing mode $-\alpha_I$ are shown as a function of $(H - \sqrt{\eta_r})$ by the solid lines in figures 13, 14 and 15. It can be seen that the characteristics of the most unstable mode in the limit $H \gg 1$ are identical to those for $\eta_r = 1$. The gel viscosity does not affect the stability characteristics for $H \gg 1$ because the dissipation of energy in the gel in this limit is small compared to the dissipation in the fluid.

Table II.

Regime	H_{min}	γ_c	k_c	$-\alpha_I$
$H \gg 1$		H^{-1}	H^{-1}	H^{-2}
$\eta_r = 1$ $T = 0$	1	$(H-1)^{-1/2}$	1.05	$(H-1)^{-1/2}$
$\eta_r = 1$ $T > 0$	1	$T^{1/4}(H-1)^{-3/4}$	$T^{-1}(H-1)^{1/4}$	$(H-1)^{-1/2}$
$\eta_r > 1$ $T \geqslant 0$	$\sqrt{\eta_r}$	$(H-\sqrt{\eta_r})^{-1}$	$(H-\sqrt{\eta_r})^{1/2}$	$(H-\sqrt{\eta_r})^{-1/2}$
$\eta_r < 1$ $T = 0$	0	Finite (Fig. 19)	H^{-1} (Fig. 20)	Finite
$\eta_r < 1$ $T \to \infty$	Fig. 21	$(H-H_{min})^{-1/2}$	$T^{-1/2}$ (Fig. 22)	$(H-H_{min})^{-1/2}$

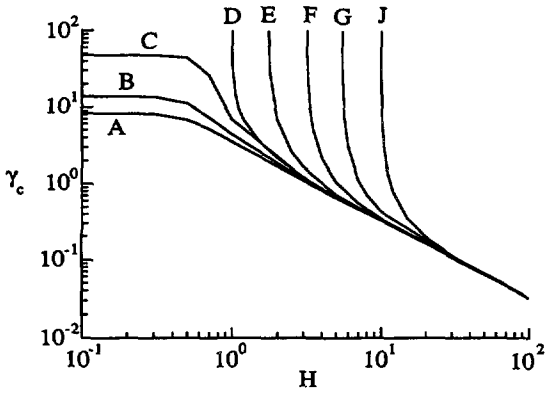

Fig. 12.

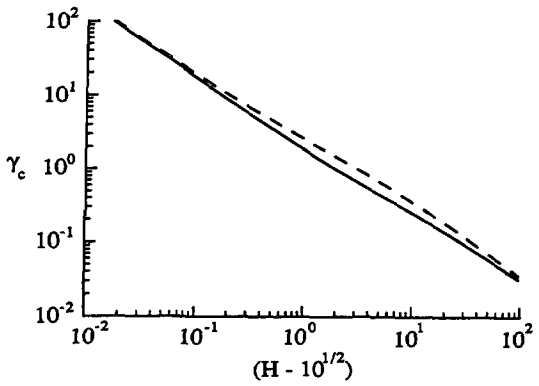

Fig. 13.

Fig. 12. — Critical strain rate γ as a function of H. (A) $\eta_r = 0$; (B) $\eta_r = 0.3$; (C) $\eta_r = 0.7$; (D) $\eta_r = 1.0$; (E) $\eta_r = 3.0$; (F) $\eta_r = 10.0$; (G) $\eta_r = 30.0$; (J) $\eta_r = 100.0$.

Fig. 13. — The critical strain rate, γ_c, required for unstable modes as a function of $(H - 10^{1/2})$ for $\eta_r = 10$. (Solid line) $T = 0$; (Broken line) $T = 100$.

In the limit $H - \sqrt{\eta_r} \ll 1$, the critical strain rate γ_c increases proportional to $(H - \sqrt{\eta_r})^{-1}$, while the critical wave number k_c is proportional to $(H - \sqrt{\eta_r})^{1/2}$, and the critical wave number decreases to zero for $H \to \eta_r$. The frequency of the most unstable mode $-\alpha_I$ is proportional to $(H - \sqrt{\eta_r})^{-1/2}$ in this limit.

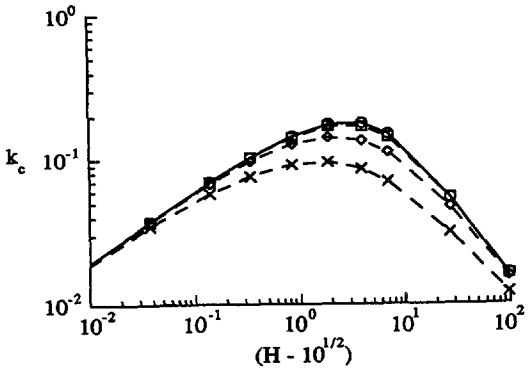

Fig. 14.

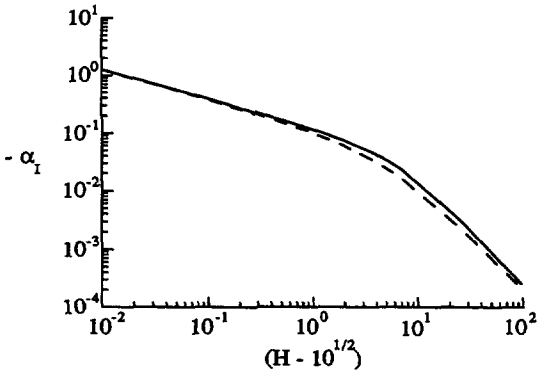

Fig. 15.

Fig. 14. — Wave number of the marginally stable mode, k_{max}, as a function of $(H - 10^{1/2})$ and $\eta_r = 10$. (○) $T = 0$; (□) $T = 1$; (◇) $T = 10$; (×) $T = 100$.

Fig. 15. — Frequency of the marginally stable mode, $-\alpha_I$, as a function of $(H - 10^{1/2})$ and $\eta_r = 10$. (Solid line) $T = 0$; (Broken line) $T = 100$.

The effect of surface tension on the properties of the most unstable mode is shown by the broken lines in figures 13, 14 and 15. We see that surface tension does not affect the stability characteristics in either limit $H \gg 1$ or $(H - \sqrt{\eta_r}) \ll 1$ because the wave number of the most unstable mode approaches zero in both limits. In the intermediate regime, an increase in the surface tension tends to increase γ_c and decrease k_c and $-\alpha_I$. The results for $\eta_r > 1$ are summarized in table II.

4.3 $\eta_r < 1$. — Returning to figure 12, we see that the critical strain rate approaches a finite value in the limit $H \to 0$ for $\eta_r < 1$ and $T = 0$. To examine this further, the solid lines in figures 16, 17 and 18 show the critical strain rate γ_c, the critical wave number k_c and the frequency of the most unstable mode $-\alpha_I$ as a function of H at $\eta_r = 1$ and $T = 0$. The characteristics of the most unstable mode in the limit $H \gg 1$ are identical to those for $\eta_r \geq 1$ for the reasons mentioned in the previous section. In the limit $H \ll 1$, we see that the critical strain rate approaches a finite value γ_{c0} and the critical wave number k_{c0} increases

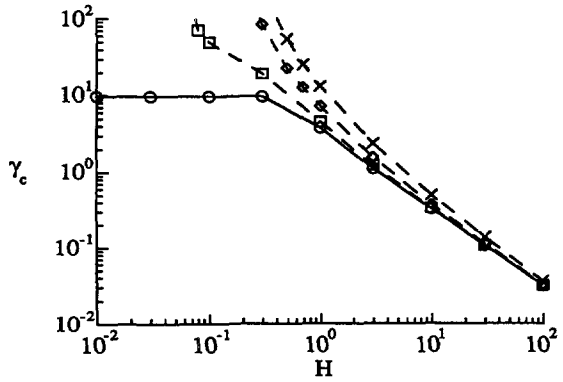

Fig. 16. — The critical strain rate, γ_c, required for unstable modes as a function of H for $\eta_r = 0.1$. (○) $T = 0$; (□) $T = 1$; (◇) $T = 10$; (×) $T = 100$.

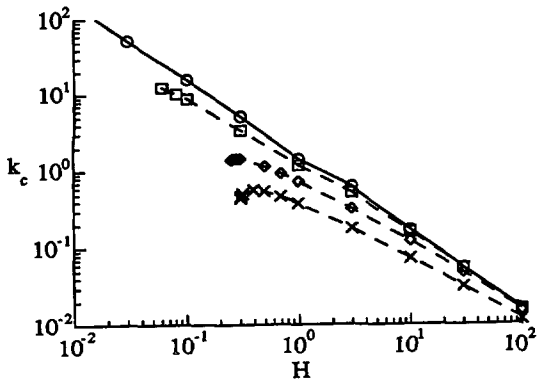

Fig. 17.

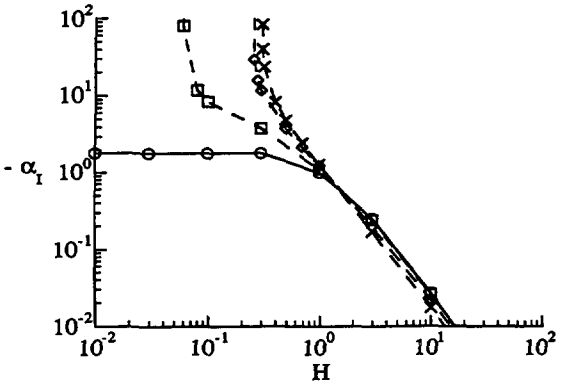

Fig. 18.

Fig. 17. — Wave number of the marginally stable mode, k_{max}, as a function of H and $\eta_r = 0.1$. (○) $T = 0$; (□) $T = 1$; (◇) $T = 10$; (×) $T = 100$.

Fig. 18. — Frequency of the marginally stable mode, $-\alpha_I$, as a function of H and $\eta_r = 0.1$. (○) $T = 0$; (□) $T = 1$; (◇) $T = 10$; (×) $T = 100$.

proportional to H^{-1}. The critical strain rate γ_{c0}, which is shown as a function of $(1 - \eta_r)$ in figure 19, is 8.219 at $\eta_r = 0$ and increases proportional to $(1 - \eta_r)^{-3/2}$ for $\eta_r \to 1$. The product of the critical wave number and the gel thickness, Hk_{c0}, shown in figure 20, is 1.515 at $\eta_r = 0$, and increases proportional to log $(1 - \eta_r)$ for $\eta_r \to 1$. Finally, we observe that the frequency of the most unstable mode $-\alpha_I$ is proportional to γ_c for $\eta_r < 1$ and $(H/R) \to 0$.

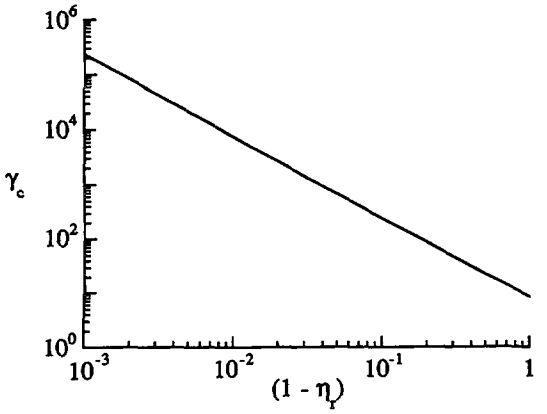

Fig. 19.

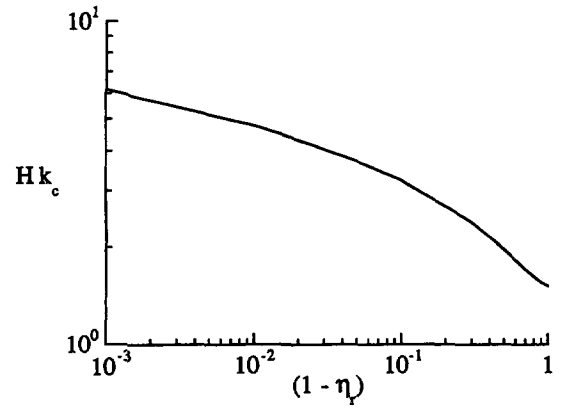

Fig. 20.

Fig. 19. — Critical strain rate γ_c as a function of $(1 - \eta_r)$ at $H = 0$ and $T = 0$.

Fig. 20. — Hk_c as a function of $(1 - \eta_r)$ in the limit $H \to 0$ and $T = 0$.

The broken lines in figures 16, 17 and 18 show that a variation in the surface tension has a dramatic effect on the characteristics of the most unstable wave for $\eta_r < 1$. The critical strain rate diverges at a finite value of H_{min} which depends on the surface tension T for $T \neq 0$, while the critical wave number approaches a finite value at H_{min}. The frequency of the

most unstable mode – α_I increases proportional to γ_c near H_{min}. It is of interest to determine the minimum value of the gel thickness required for unstable modes, H_{min}, in the limit of high surface tension $T \to \infty$, since the stabilising effect of the surface tension is maximum in this limit. This was found by calculating H_{min} for increasing values of T, usually up to 10^5, until the variation in H_{min} was less than 0.01 of its value when T was increased by a factor of 10. The results of this calculation, which are shown in figure 21, indicate that H_{min} approaches 1 for $\eta_r \to 1$ (as might be expected from the results for $\eta_r = 1$), and it decreases proportional to $\eta_r^{1/2}$ for $\eta_r \to 0$. The critical strain rate γ and the frequency of the most unstable mode – α_I increase proportional to $(H - H_{min})^{-1/2}$ for $H \to H_{min}$, but the wave number of the most unstable mode, k_c, remains finite in this limit. The limiting value of k_c decreases proportional to $T^{-1/2}$ for $T \to \infty$, and figure 22 shows $T^{1/2} k_c$ as a function of η_r. This increases proportional to $\eta_r^{-1/2}$ for $\eta_r \to 0$, and decreases to zero at $\eta_r = 1$. The above results are summarized in table II.

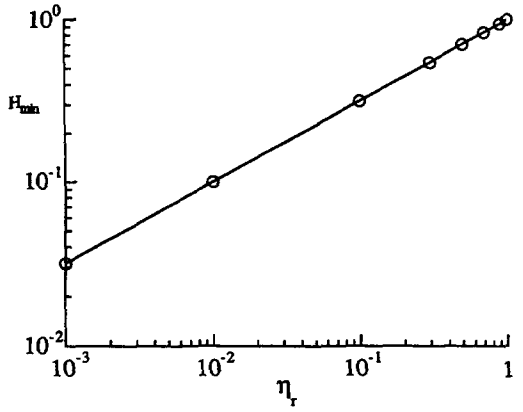

Fig. 21.

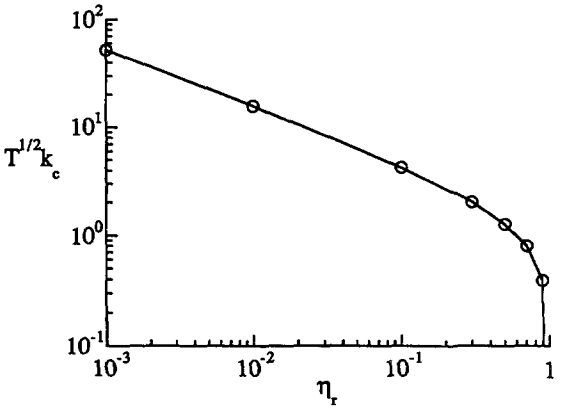

Fig. 22.

Fig. 21. — H_{min}, the minimum gel thickness required for the presence of unstable modes, as a function of η_r in the limit $T \to \infty$.

Fig. 22. — $T^{1/2} k_c$ as a function of η_r in the limit $T \to \infty$.

5. Discussion.

In this section, we first recall some interesting qualitative aspects of the instability, and then compare the results with some experimental observations. One interesting feature is that the inertia of the fluid or elastic medium is not required to produce unstable modes. In Newtonian fluids the instabilities are associated with the fluid inertia, since in the absence of inertia the Navier-Stokes equations are quasi-steady and do not explicitly depend on time. The instability of the interface between two viscoelastic fluids [9] has been attributed to a jump in the first normal stress at the surface. In the present case, however, we observe an instability at an interface between an elastic medium and a fluid in the absence of inertia and normal stress discontinuities. The time dependence enters through the elastic term in the constitutive equation of the gel, and the interplay of the elastic and viscous effects is responsible for inducing interfacial instabilities.

The interface becomes unstable when the strain rate in the fluid increases beyond a critical value. The mean flow and perturbation fields are coupled through the boundary condition for

the velocity in the x direction (29). The term proportional to γ in (29) causes a transport of energy from the mean flow to the velocity perturbations, which tends to destabilise the interface. The rate of transport of energy is proportional to the product of γ and the normal displacement at the interface. The coupling between the mean flow and perturbation field in this case is similar to that in the case of vertically stratified inviscid fluids in relative horizontal motion, which gives rise to the Kelvin-Helmoltz instability [17], though in the present case the instability is caused by a discontinuity in the strain rate in the mean flow and not the velocity itself.

The critical strain rate γ_c, which is the minimum strain rate for the onset of instability, depends on the ratio of the thickness of the gel and fluid, H, the ratio of the gel and fluid viscosities, η_r, and the ratio of the surface tension and elastic forces, $T = (\Gamma/ER)$, where Γ is the surface tension of the gel-fluid interface. In the limit $H \to \infty$, the characteristics of the most unstable mode are independent of T and η_r. The critical strain rate γ_c and the wave number of the most unstable mode k_c decrease proportional to H^{-1} in this limit, while the frequency of the most unstable mode decreases proportional to H^{-2}. The reason for the universal nature of the instability can be understood as follows — in the limit $H \gg 1$, the strain rate and the viscous dissipation in the fluid are large compared to that in the gel, so the rate of dissipation of energy is controlled by the fluid dynamics alone and independent of the gel viscosity. Also, the properties of the most unstable mode are independent of T because the wavelength of the fastest growing mode increases proportional to H for $H \gg 1$, and the stress due to surface tension decreases as the wavelength increases.

For $H \sim 1$, the most unstable mode has qualitatively different characteristics for the cases $\eta_r < 1$, $\eta_r = 1$ and $\eta_r > 1$. For $\eta_r > 1$, we find that the interface is always stable for $H < \sqrt{\eta_r}$, while there are unstable modes for $H > \sqrt{\eta_r}$. In the limit $H \to \sqrt{\eta_r}$, the wave number of the most unstable mode, k_c, decreases proportional to $(H - \sqrt{\eta_r})^{1/2}$, and consequently the effect of surface tension becomes negligible in this limit. The critical strain rate γ_c diverges proportional to $(H - \sqrt{\eta_r})^{-1}$ and the frequency of the most unstable mode diverges proportional to $(H - \sqrt{\eta_r})^{-1/2}$. In between the two limits, an increase in the surface tension tends to reduce the wave number k_c and the frequency of the most unstable mode $-\alpha_I$, and increase the critical strain rate γ_c.

When the gel and fluid viscosities are equal ($\eta_r = 1$), the surface is always stable for $H < 1$. Though this minimum value of H for unstable modes is independent of surface tension, the characteristics of the unstable modes are a strong function of T. In the limit $H \to 1$, we find that $\gamma_c \propto (H-1)^{-1/2}$, $k_c \to 1.05$ and $-\alpha_I \propto (H-1)^{-1/2}$ for $T = 0$; and $\gamma_c \propto T^{1/4}(H-1)^{-3/4}$, $k_c \propto T^{-1}(H-1)^{1/4}$ and $-\alpha_I \propto (H-1)^{-1/2}$. The presence of surface tension increases the rate of divergence of the critical strain rate, and reduces the wave number of the most unstable mode from a finite value for $T = 0$ to $T^{-1}(H-1)^{1/4}$ for $T > 0$. Surface tension has little effect on the frequency of the most unstable mode.

For $\eta_r < 1$, the surface tension changes H_{min}, the minimum value of H required for the presence of unstable modes. In the absence of surface tension ($T = 0$), there are unstable modes even in the limit $H \to 0$, and the critical strain rate γ_c remains finite in this limit. The wave number of the most unstable mode, k_c, diverges proportional to H^{-1} and the frequency of the most unstable mode remains finite. In the presence of surface tension ($T > 0$), the critical strain rate diverges at a finite value of $H = H_{min}$, and the rate of divergence is proportional to $(H - H_{min})^{-1/2}$. In this case, the wave number of the most unstable mode is finite, but its frequency diverges proportional to $(H - H_{min})^{-1/2}$

Thus, we see that though the qualitative effect of an increase in the viscosity ratio η_r and surface tension T is to increase the critical strain rate and reduce the wave number of the most unstable modes, there is a rich variety in the characteristics of the instability that would

not be captured by less detailed analyses which do not include the gel and fluid dynamics in an essentially exact fashion. We are not aware of any experiments for $H \sim 1$ that could be compared with the theory, but the experiments of Krindel and Silberberg [18] are in qualitative agreement with our results in the limit $H \gg 1$. Krindel and Silberberg [18] studied the flow of a Newtonian fluid through a tube whose walls were made of a polymer gel, and the thickness of the walls was large compared to the radius of the tube. They observed that there was an anomalous increase in the drag force for $\mathrm{Re} > \mathrm{Re}_G$, and this increase was attributed to a transition from a laminar to a turbulent flow, where $\mathrm{Re}_G = (ER^2 \rho/4 H\eta^2)$. Our analysis predicts an instability for $\gamma > 3.2 H^{-1}$, which is equivalent to $\mathrm{Re} > 3.2\, \mathrm{Re}_G$ in the notation of Krindel and Silberberg. Thus, we see that our prediction of the transition Reynolds number is in agreement with the observation of Krindel and Silberberg, except for the constant prefactor. This difference may be due to the difference in the geometry. We note that the difference in the mean flow profile does not affect the results of our analysis, because the only coupling between the mean flow and the fluctuations is *via* the strain rate at the wall. Therefore, the results for a Poiseuille flow (used by Krindel and Silberberg) will be the same as that for the Couette flow studied here as long as the strain rate at the surface is the same.

Acknowledgments.

Acknowledgment is made to the donors of the Petroleum Research Fund, administered by the Americal Chemical Society, for support of this research (V. K. and G. F.). P. P. is grateful to IBM and DOE (DE-FG03-87ER45288) for financial support.

Appendix A.

In this appendix, we present the detailed derivation of the characteristic equation for the growth rate of perturbations at the interface between the elastic medium and the fluid for the case $\eta_r = 1$ and $T = 0$. The eigenfunctions for the displacement field, $\tilde{u}_z$ and $\tilde{u}_x$, are calculated from the mass and momentum equations (21), (22) and (23). The eigen functions that are consistent with the boundary conditions at $z = -H$ (4) are :

$$\tilde{u}_z = A_1\{\exp(kz) - [1 + 2k(z + H)]\exp(-2Hk - kz)\} + \\ + A_2\{[kz]\exp(kz) + [k(2Hk(H + z) - z)]\exp(-2Hk - kz)\} \quad (A.1)$$

$$\tilde{u}_x = iA_1\{\exp(kz) + [-1 + 2k(z + H)]\exp(-2Hk - kz)\} + \\ + iA_2\{[1 + kz]\exp(kz) - [1 + 2Hk(Hk + kz - 1) - kz]\exp(-2Hk - kz)\} . \quad (A.2)$$

The displacement field at the interface $z = 0$ can be expressed in the following compact form :

$$\begin{pmatrix} \tilde{u}_z \\ \tilde{u}_x \end{pmatrix} = M_{ug} \begin{pmatrix} A_1 \\ A_2 \end{pmatrix} \quad (A.3)$$

where the matrix M_{ug} is given by :

$$\begin{aligned} M_{ug11} &= \{1 - [1 + 2Hk]\exp(-2Hk)\} \\ M_{ug12} &= \{[2(Hk)^2]\exp(-2Hk)\} \\ M_{ug21} &= i\{1 + [2Hk - 1]\exp(-2Hk)\} \\ M_{ug22} &= i\{1 - [1 - 2Hk + 2(Hk)^2]\exp(-2Hk)\} . \end{aligned} \quad (A.4)$$

The shear stress and normal stress at the interface $z = 0$ are calculated using (27). These can be

expressed in the following form :

$$\begin{pmatrix} \tilde{\sigma}_{zz} \\ \tilde{\sigma}_{xz} \end{pmatrix} = M_{sg} \begin{pmatrix} A_1 \\ A_2 \end{pmatrix} \tag{A.5}$$

where

$$\begin{aligned} M_{sg11} &= 2k(1+\alpha)[1+(1+2Hk)\exp(-2Hk)] \\ M_{sg12} &= -4k(1+\alpha)[(Hk)^2\exp(-2Hk)] \\ M_{sg21} &= 2ik(1+\alpha)[1+(1-2Hk)\exp(-2Hk)] \\ M_{sg22} &= 2ik(1+\alpha)[1+(1-2Hk+2(Hk)^2)\exp(-2Hk)] \,. \end{aligned} \tag{A.6}$$

The eigen functions for the fluid velocity field are determined from the linearised Stokes equations (24), (25) and (26). The eigen functions that are consistent with the boundary conditions at $z = 1(8)$ are :

$$\begin{aligned} \tilde{v}_z = B_1\{\exp(kz) - [1-2k(1-z)]\exp(2k-kz)\} + \\ + B_2\{[kz]\exp(kz) + [k(2k(1-z)-z)]\exp(2k-kz)\} \end{aligned} \tag{A.7}$$

$$\begin{aligned} \tilde{v}_x = iB_1\{\exp(kz) - [1+2k(1-z)]\exp(2k-kz)\} + \\ + iB_2\{[1+kz]\exp(kz) - [1+2k(1+k-kz)-kz]\exp(2k-kz)\} \,. \end{aligned} \tag{A.8}$$

The fluid velocity at the interface $z = 0$ can be expressed in the following compact form :

$$\begin{pmatrix} \tilde{v}_z \\ \tilde{v}_x \end{pmatrix} = M_{vf} \begin{pmatrix} B_1 \\ B_2 \end{pmatrix} \tag{A.9}$$

where

$$\begin{aligned} M_{vf11} &= 1 - [1-2k]\exp(2k) \\ M_{vf12} &= 2k^2\exp(2k) \\ M_{vf21} &= i\{1 - [1+2k]\exp(2k)\} \\ M_{vf22} &= i\{1 - [1+2k+2k^2]\exp(2k)\} \,. \end{aligned} \tag{A.10}$$

The shear and normal stresses due to the fluid flow can be calculated using (28), and these have the following values at the interface $z = 0$:

$$\begin{pmatrix} \tilde{\tau}_{zz} \\ \tilde{\tau}_{xz} \end{pmatrix} = M_{sf} \begin{pmatrix} B_1 \\ B_2 \end{pmatrix} \tag{A.11}$$

where

$$\begin{aligned} M_{sf11} &= 2k + 2k[1-2k]\exp(2k) \\ M_{sf12} &= -4k^3\exp(2k) \\ M_{sf21} &= i\{2k + 2k[1+2k]\exp(2k)\} \\ M_{sf22} &= i\{2k + 2k[1+2k+2k^2]\exp(2k)\} \,. \end{aligned} \tag{A.12}$$

The matching conditions for the velocity and stress at the interface, (29) and (30), give us the following relations :

$$\alpha\{M_{ug11}A_1 + M_{ug12}A_2\} = M_{vf11}B_1 + M_{vf12}B_2$$

$$\begin{aligned}
&\alpha\{M_{ug21}A_1 + M_{ug22}A_2\} - \gamma\{M_{ug11}A_1 + M_{ug12}A_2\} = M_{vf21}B_1 + M_{vf22}B_2 \\
&M_{sg11}A_1 + M_{sg12}A_2 = M_{st11}B_1 + M_{sf12}B_2 \\
&M_{sg21}A_1 + M_{sg22}A_2 = M_{sf21}B_1 + M_{sf22}B_2 .
\end{aligned} \tag{A.13}$$

After solving the above equations for the four constants A_1, A_2, B_1 and B_2, we get the following characteristic equation :

$$a\alpha^2 + (b_1 + i\gamma b_2)\alpha + c_1 + i\gamma c_2 = 0 \tag{A.14}$$

where

$$\begin{aligned}
a = &-4[1 - \exp(2k(1+H)) + 2k(1+H)\exp(k(1+H))] \\
&\times [1 - \exp(2k(1+H)) - 2k(1+H)\exp(k(1+H))]
\end{aligned} \tag{A.15}$$

$$\begin{aligned}
b_1 = &4\{-1 - \exp(4k(1+H)) + [1+2k^2][\exp(2k) + \exp(2k+4Hk)] - \\
&- [1+2(Hk)^2][\exp(2Hk) + \exp(4k+2Hk)] \\
&+ 2[1+2k^2+4Hk^2+2(Hk)^2]\exp(2k+2Hk)\}
\end{aligned} \tag{A.16}$$

$$\begin{aligned}
b_2 = &4\{k^2[\exp(2k) - \exp(2k+4Hk)] + (Hk)^2[\exp(2Hk) - \exp(4k+2Hk)] + \\
&+ 4Hk^3[1+H]\exp(2k+2Hk)\}
\end{aligned} \tag{A.17}$$

$$\begin{aligned}
c_1 = &[1 - \exp(2k) + 2k\exp(k)][-1 + \exp(2k) + 2k\exp(k)] \times \\
&\times [1 + \exp(4Hk) + (2 + 4(Hk)^2)\exp(2Hk)]
\end{aligned} \tag{A.18}$$

$$\begin{aligned}
c_2 = &-4k^2\{\exp(2k+4Hk) - \exp(2k) + H^2[\exp(4k+2Hk) - \exp(2Hk)] \\
&- 4Hk[1+H]\exp(2k+2Hk)\} .
\end{aligned} \tag{A.19}$$

Though the analytical expressions for the solutions of this quadratic equation are unwieldly, the roots can be numerically calculated quite easily, and the characteristics of the root with the larger real part are discussed in section 4.

References

[1] Silberberg A., Physico-chemical hydrodynamics in turbulent flows close to an interface, *Physico Chemical Hydrodynamics* **9** (1987) 419.

[2] Klein J., Perahia D. and Warburg S., Forces between polymer — bearing surfaces undergoing shear, *Nature* **143** (1991) 352.

[3] Gupta A. S., Stability of a visco-elastic liquid film flowing down an inclined plane, *J. Fluid Mech.* **28** (1967) 17.

[4] Shaqfeh E. S. G., Larson R. G. and Fredrickson G. H., The stability of gravity deriven viscoelastic film — flow at low to moderate Reynolds number, *J. Non-Newtonian Fluid Mech.* **21** (1989) 87.

[5] Yih C. S., Instability due to viscosity stratification, *J. Fluid Mech.* **27** (1970) 337.

[6] Hooper A. and Boyd W. G., Shear flow instability at the interface between two viscous fluids, *J. Fluid Mech.* **128** (1983) 507.

[7] Waters N. D. and Keely A. M., The stability of two stratified non-Newtonian liquids a in Couette flow, *J. Non-Newtonian Fluid Mech.* **24** (1987) 161.

[8] Renardy Y., Stability of the interface in two-layer Couette flow of upper convected Maxwell liquids, *J. Non-Newtonian Fluid Mech.* **28** (1988) 99.

[9] Chen K. P., Interfacial instability due to the elastic stratification in concentric coextrusion of two viscoelastic fluids, *J. Non-Newtonian Fluid Mech.* **40** (1991) 155.

[10] Landau L. D. and Lifshitz E. M., Theory of Elasticity (Pergamon, New York, 1989), Chap. 1.

[11] Harden J. L., Pleiner P. and Pincus P. A., Hydrodynamic surface modes on concentrated polymer solutions and gels, *J. Chem. Phys.* **94** (1991) 5208.
[12] de Gennes P.-G., Dynamics of entangled polymer solutions. Part 1 : The Rouse model, *Macromolecules* **9** (1976) 594.
[13] Kumaran V., Surface modes on a polymer gel of finite thickness, *J. Chem. Phys.* **98** (1993) 3429.
[14] Riley J., Gad-el-Hak M. and Metcalfe R. W., Compliant coatings, *Annu. Rev. Fluid Mech.* **20** (1988) 393.
[15] Carpenter P. W. and Garrad A. D., The hydrodynamic stability of flow over Kramer type compliant surfaces. Part 1. Tollmein-Schlichting instabilities, *J. Fluid Mech.* **155** (1985) 465.
[16] Carpenter P. W. and Garrad A. D., The hydrodynamic stability of flow over Kramer type compliant surfaces. Part 2. Tollmein-Schlichting instabilities, *J. Fluid Mech.* **170** (1986) 199.
[17] Chandrasekhar S., Hydrodynamic and Hydromagnetic Stability (Dover, 1981) Chapter 11.
[18] Krindel P. and Silberberg A., Flow through gel-walled tubes, *J. Colloid Interface Sci.* **71** (1979) 39.